Physics of the Earth and Planetary Interiors 269 (2017) 91–97

Contents lists available at ScienceDirect

Physics of the Earth and Planetary Interiors

journal homepage: www.elsevier.com/locate/pepi

Elasticity of phase-Pi ($Al_3Si_2O_7(OH)_3$) – A hydrous aluminosilicate phase

Ye Peng [a], Mainak Mookherjee [a,*], Andreas Hermann [b], Suraj Bajgain [a], Songlin Liu [a,c], Bernd Wunder [d]

[a] Earth Materials Laboratory, Department of Earth, Ocean and Atmospheric Sciences, Florida State University, Tallahassee, FL 32306, USA
[b] School of Physics and Astronomy, James Clerk Maxwell Building, The University of Edinburgh, Edinburgh EH9 3FD, UK
[c] CAS Key Laboratory of Crust-Mantle Materials and Environments, School of Earth and Space Sciences, University of Science and Technology of China, Hefei, China
[d] GFZ, German Research Center for Geoscience, 14473 Potsdam, Germany

ARTICLE INFO

Article history:
Received 27 January 2017
Received in revised form 11 May 2017
Accepted 22 May 2017
Available online 24 May 2017

Keywords:
High-pressure
Phase-Pi
Equation of state
Elasticity
Anisotropy
Subduction zone

ABSTRACT

Phase-Pi ($Al_3Si_2O_7(OH)_3$) is an aluminosilicate hydrous mineral and is likely to be stable in hydrated sedimentary layers of subducting slabs. Phase-Pi is likely to be stable between the depths of 60 and 200 km and is likely to transport water into the Earth's interior. Here, we use *first principles* simulations based on density functional theory to explore the crystal structure at high-pressure, equation of state, and full elastic stiffness tensor as a function of pressure. We find that the pressure volume results could be described by a finite strain fit with V_0, K_0, and K'_0 being 310.3 Å^3, 133 GPa, and 3.6 respectively. At zero pressure, the full elastic stiffness tensor shows significant anisotropy with the diagonal principal components C_{11}, C_{22}, and C_{33} being 235, 292, 266 GPa respectively, the diagonal shear C_{44}, C_{55}, and C_{66} being 86, 92, and 87 GPa respectively, and the off-diagonal stiffness C_{12}, C_{13}, C_{14},C_{15}, C_{16}, C_{23}, C_{24}, C_{25}, C_{26}, C_{34}, C_{35}, C_{36}, C_{45}, C_{46}, and C_{56} being 73, 78, 6, −30, 15, 61, 17, 2, 1, −13, −15, 6, 3, 1, and 3 GPa respectively. The zero pressure, shear modulus, G_0 and its pressure derivative, $G_{0\prime}$ are 90 GPa and 1.9 respectively. Upon compression, hydrogen bonding in phase-Pi shows distinct behavior, with some hydrogen bonds weakening and others strengthening. The latter eventually undergo symmetrization, at pressure greater (>40 GPa) than the thermodynamic stability of phase-Pi. Full elastic constant tensors indicate that phase-Pi is very anisotropic with AV_P ~22.4% and AV_S ~23.7% at 0 GPa. Our results also indicate that the bulk sound velocity of phase-Pi is slower than that of the high-pressure hydrous aluminosilicate phase, topaz-OH.

1. Introduction

Water plays an important role in the long-term sustenance of solid Earth activities. For instance, water lowers the melting temperatures of silicate rocks and could lead to melting in the deep Earth (Hirschmann, 2006). Water, present in trace quantities within nominally anhydrous minerals, affects the transport properties including rheology (*e.g.*, Mei and Kohlstedt, 2000), viscosity (*e.g.*, Ichikawa et al., 2015) and electrical conductivity (*e.g.*, Wang et al., 2006). Water is transported into the deep Earth via subduction of hydrated lithosphere containing hydrous mineral phases (Kawamoto, 2006). These minerals are distinct from the nominally anhydrous phases and contain structurally bound hydroxyl groups i.e., OH^- groups occur in well-defined crystallographic sites (Smyth, 2006).

It is well known that sedimentary layers are typically less dense compared to the subducting oceanic crust and lithospheric mantle and hence may not readily subduct. However, based on geochemical evidences i.e., ^{10}Be signature in island arc volcanism, it is well known that sedimentary layers do undergo subduction and are recycled back at arc (Tera et al., 1986; Morris and Tera, 1989; White and Dupre, 1986). Estimates based on deep sea drilling suggest that the amount of sediment subduction is of the order of ~1–2 × 10^{15} g/yr (Plank and Langmuir, 1993; Rea and Ruff, 1996). Among the sediments, contribution from terrigenous sediments dominates. Contribution from carbonate sediment is minor (Rea and Ruff, 1996). The sedimentary layer also helps to subduct water on the order of 1 × 10^{15} g/year (Rea and Ruff, 1996). Part of the subducted water is recycled back through island arc volcanism, however a part of the water is carried into the deep Earth. The water helps in hydrating the subducting lithosphere and the overlying mantle. While the net water contribution from oceanic crust is likely to be greater than the sediments (Peacock, 1990), owing to the greater thermal stability of the minerals stabilized in sedimentary layer, they may be effective in transporting water into the deep Earth in warmer subduction zones (Ono, 1998).

The mineralogy of subducted sediments can be understood within a simplified ternary system, where the end member chemical components are represented by- Al_2O_3-SiO_2-H_2O (ASH)

* Corresponding author.
E-mail address: mmookherjee@fsu.edu (M. Mookherjee).

http://dx.doi.org/10.1016/j.pepi.2017.05.016
0031-9201/

(Peacock, 1990; Ono, 1999; Schmidt et al., 1998; Schreyer, 1995; Daniels and Wunder, 1993; Wunder et al., 1993a,b). Several hydrous mineral phases are stable in the ASH ternary system. These include gibbsite ($Al(OH)_3$), diaspore (AlOOH), kaolinite ($Al_2Si_2O_5(OH)_4$), topaz-OH ($Al_2SiO_4(OH)_2$), phase-Pi ($Al_3Si_2O_7(OH)_3$), phase Egg ($AlSiO_3(OH)$), and dense high-pressure phases such as δ-AlOOH. Among these various phases, almost nothing is known about the high-pressure behavior of phase-Pi. However, it is likely to play an important role in transporting water into the deep Earth. High-pressure phase relations have shown that phase-Pi is stable between 2 and 7 GPa (Wunder et al., 1993a,b). In this study, we explore the behavior of phase-Pi at high-pressure. We have used *first principles* simulations to explore how pressure affects the crystal structure and proton environments, equation of state, full elastic constant tensor and elastic anisotropy at high-pressures.

2. Method

In this study, we examined the crystal structure, equation of state, and elasticity of phase-Pi ($Al_3Si_2O_7(OH)_3$), using static density functional theory calculations using the Vienna ab-initio simulation package (VASP) (Hohenberg and Kohn, 1964; Kohn and Sham, 1965; Kresse and Hafner, 1993; Kresse and Furthmüller, 1996a,b; Kresse and Joubert, 1999). We used generalized gradient approximation (GGA) (PBE: Perdew et al., 1996) and the highly accurate projector augmented wave method (PAW) as implemented in VASP (Kresse and Joubert, 1999). It is known that PBE often describes the energetics and elasticity of hydrous phases better than the local density approximation (LDA) (Mookherjee and Mainprice, 2014; Mookherjee and Tsuchiya, 2015). We performed a series of convergence tests by varying the energy cutoff and *k*-

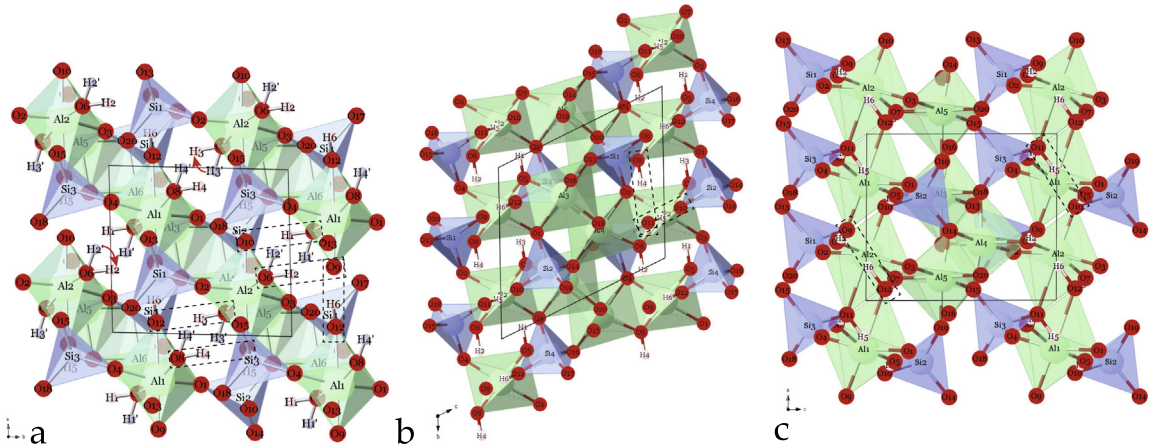

Fig. 1. Crystal structure of phase-Pi: (a-c) represents the projection down the *c*-, *a*-, and *b*- crystallographic axes respectively. The light-blue polyhedral units represent SiO_4 tetrahedral units. The light green polyhedral units represent AlO_6 octahedral units. The red and white spheres are oxygen and hydrogen atoms respectively. The grey atoms denote the starting guesses for the hydrogen atom positions H1′, H2′, H3′, and H4′ based on single crystal X-ray diffraction (Daniels and Wunder, 1996). The flip in positions from H1′, H2′, H3′, and H4′ to the relaxed positions of H1, H2, H3, and H4 is shown by curved and dashed (red) arrows. The protons and related oxygen atom pairs are shown by the dashed rectangles, there are six such O-H···O units, i.e., O5-H1---O10; O6-H2---O11; O7-H3---O12; O8-H4---O11; O11-H5---O10; and O12-H6---O9.

Table 1
Fractional coordinates of oxygen and hydrogen atoms for the starting configuration and fully relaxed crystal structure of phase Pi.

Atom/Label	Structural Parameters: Starting Guess[#]						Structural Parameters: Fully Relaxed[*]					
	Fractional coordinates			$d_{O\text{-}H}$	$d_{H\text{---}H}$	$d_{H\text{---}O}$	Fractional coordinates			$d_{O\text{-}H}$	$d_{H\text{---}H}$	$d_{H\text{---}O}$
	x	y	z	[Å]			x	y	z	[Å]		
O5	0.6261	0.1399	0.1535				0.6344	0.1342	0.1528			
H1	0.4830	0.0881	0.1796	0.9840			0.6096	0.9890	0.1309	0.9980		
O6	0.3478	0.8647	0.8482				0.3512	0.8616	0.8462			
H2	0.4948	0.9130	0.8203	0.9990			0.3760	0.0069	0.8682	0.9980		
H1---O3						1.9430						
H1---O10												1.6330
H2---O4						1.9250						
H2---O11												1.6330
H1---H2					2.5026						2.5592	
O7	0.1268	0.6397	0.1496				0.1322	0.6350	0.1530			
H3	0.9855	0.5901	0.1762	0.9690			0.0983	0.4916	0.1292	0.9880		
O8	0.8487	0.3642	0.8463				0.8534	0.3609	0.8460			
H4	0.9936	0.4112	0.8222	0.9740			0.8874	0.5043	0.8699	0.9880		
H3---O1						1.9850						
H3---O12												1.6940
H4---O2						1.9770						
H4---O11												1.6940
H3---H4					2.4669						2.4433	
O11	0.9203	0.7554	0.9038				0.9206	0.7507	0.9045			
H5	0.7980	0.7508	0.9689	0.8970			0.7842	0.7602	0.9895	1.0320		
O12	0.0559	0.2424	0.0999				0.0651	0.2451	0.0945			
H6	0.1821	0.2412	0.0308	0.9250			0.2015	0.2357	0.0095	1.0320		

[#] Single Crystal X-ray Diffraction (Daniels and Wunder, 1993,1996).
[*] cif files for the relaxed crystal structures are in supplementary files.

points. We found that an energy cut-off E_{cut} = 800 eV and a k-point mesh of $3 \times 3 \times 3$ Monkhorst-Pack grid (Monkhorst and Pack, 1976) with 14 irreducible k-points is sufficient for describing the energetics of phase-Pi (Supplementary Table 1).

We determined the full elastic constant tensor by straining the lattice parameters by 1%, as outlined in previous studies (Chheda et al., 2014; Mookherjee, 2014), and used symmetric finite displacements (by 0.015 Å) to obtain the Hessian matrix and zone-center vibrational frequencies. We computed the single crystal azimuthal anisotropy for compressional (AV_P) and shear (AV_S) waves in phase-Pi using the formulation for maximum polarization anisotropy (Mainprice, 1990).

3. Results

3.1. Crystal structure

The crystal structure of phase-Pi consists of close packing layers of oxygen atoms along the (110) planes. Perpendicular to the (110) plane, there are layers of distorted eight-membered rings formed by AlO_6 units alternating with layers consisting of SiO_4 tetrahedral units (Fig. 1). The distortion of the close packing and the eight-membered rings results in a very low overall space group symmetry ($P\bar{1}$). There are six distinct proton environments where each proton is attached to an oxygen atom i.e., O5-H1, O6-H2, O7-H3, O8-H4, O11-H5, and O12-H6. The proton environments for H1,

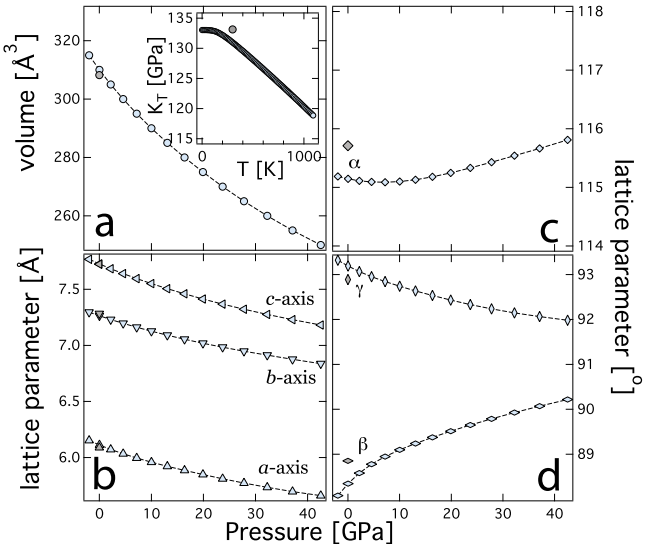

Fig. 3. (a) Pressure-volume results of phase-Pi. Inset shows the temperature dependence of the bulk modulus (K_T) (filled light blue symbol) using Gibbs2 (Otero-de-la-Roza et al., 2011) the grey filled symbol represents experimental result (Grevel et al., 2000) (b) Lattice parameters, a-, b-, and c- axes as a function of pressure. (c) Angular lattice parameters, α, (d) β, and γ as a function of pressure. Predictions from this work (light blue filled symbols) are compared to experiment (filled light grey symbols) (Daniels and Wunder, 1996).

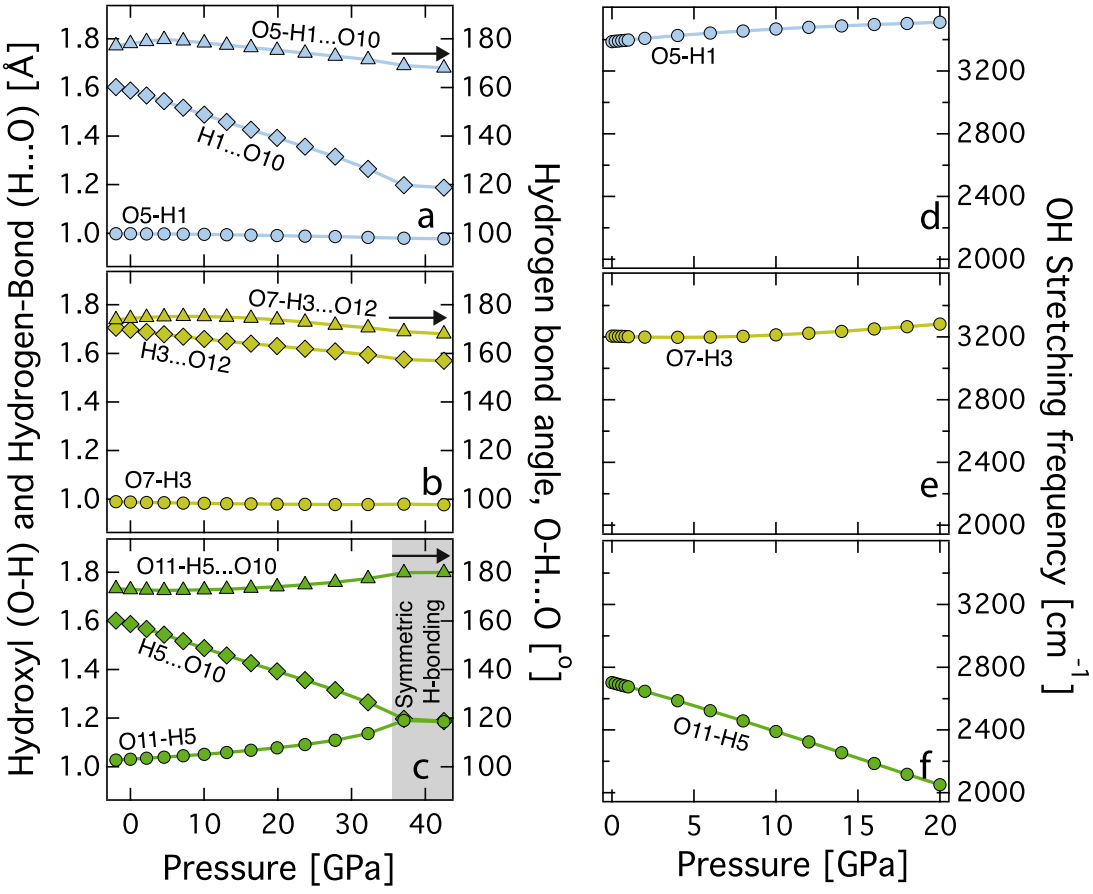

Fig. 2. There are six distinct wyckoff sites for the hydrogen atoms (Table 1). The left panel (a, b, and c) shows the evolution of O–H (filled diamonds) and H···O bonds (filled circles), and the O-H···O angles (filled triangles) upon compression. The right panel (d, e, and f) shows the evolution of the corresponding O–H stretching frequencies as a function of pressure. The magnitude and the pressure dependence of O5-H1, O7-H3, and O11-H5 are similar to O6-H2, O8-H4, and O12-H6 respectively and hence are not shown here. Two hydrogen sites H5 and H6 exhibit symmetrization of hydrogen bonding at pressures greater than 35 GPa (shaded region in light grey), i.e., beyond the thermodynamic stability of phase-Pi. As the hydrogen bond symmetrizes the O-H···O angle also becomes linear, i.e., 180°.

H2, H3, and H4 are characterized by H---H repulsion and H---O attraction. In comparison to our starting guess crystal structure based on single crystal X-ray diffraction (Daniels and Wunder, 1996), the relaxed crystal structure shows lower H---H repulsion and/or slight enhancement of the H---O attraction and hence slightly larger covalent O–H bond lengths for the H1, H2, H3, and H4 protons (Table 1, Fig. 1). Upon compression, the O-H···O hydrogen bonding in H5 and H6 is strong: the covalent bond lengths are 1.03 Å at 0 GPa and increase significantly, eventually resulting in complete symmetrization, i.e., the $d_{O\text{-}H}$ become equal to the $d_{H\cdots O}$, at around ~42 GPa. In contrast, the hydrogen bonding, O–H---O in H1, H2, H3, and H4 remains relatively weak. Unlike, O11-H5 and O12-H6, the covalent O–H bond lengths for H1, H2, H3, and H4 remain insensitive to pressures and even decrease slightly, from 0.99–1.00Å at 0 GPa to 0.97Å at 40 GPa, while the hydrogen-bonded H···O distances reduce by only 5–6% over the same pressure range. In agreement with the proton positions in the crystal structure, the O–H vibron frequencies are comparable to free hydroxyl groups at 0 GPa (3200–3400 cm^{-1}) and stiffen further under compression (3260–3510 cm^{-1} at 22 GPa) (Fig. 2). The O–H···O angle for H5 and H6 increases and becomes linear (180°) as the hydrogen bond symmetrizes. The O–H vibron modes associated with those protons are much weaker at 0 GPa (2700 cm^{-1}) and decrease rapidly under compression (down to 2050 cm^{-1} at 22 GPa), as further indication of significant hydrogen bonding that intensifies with pressure. It is known that hydrogen bond symmetrization often affects the elasticity of hydrous phases including phase-D, phase-H, and δ-AlOOH (Tsuchiya et al., 2002, 2005; Tsuchiya and Mookherjee, 2015). However, in phase-Pi the hydrogen bond symmetrization occurs at pressures much beyond its thermodynamic stability, similar to other hydrous mineral phases including the 3.65 Å phase and a high-pressure phase of brucite

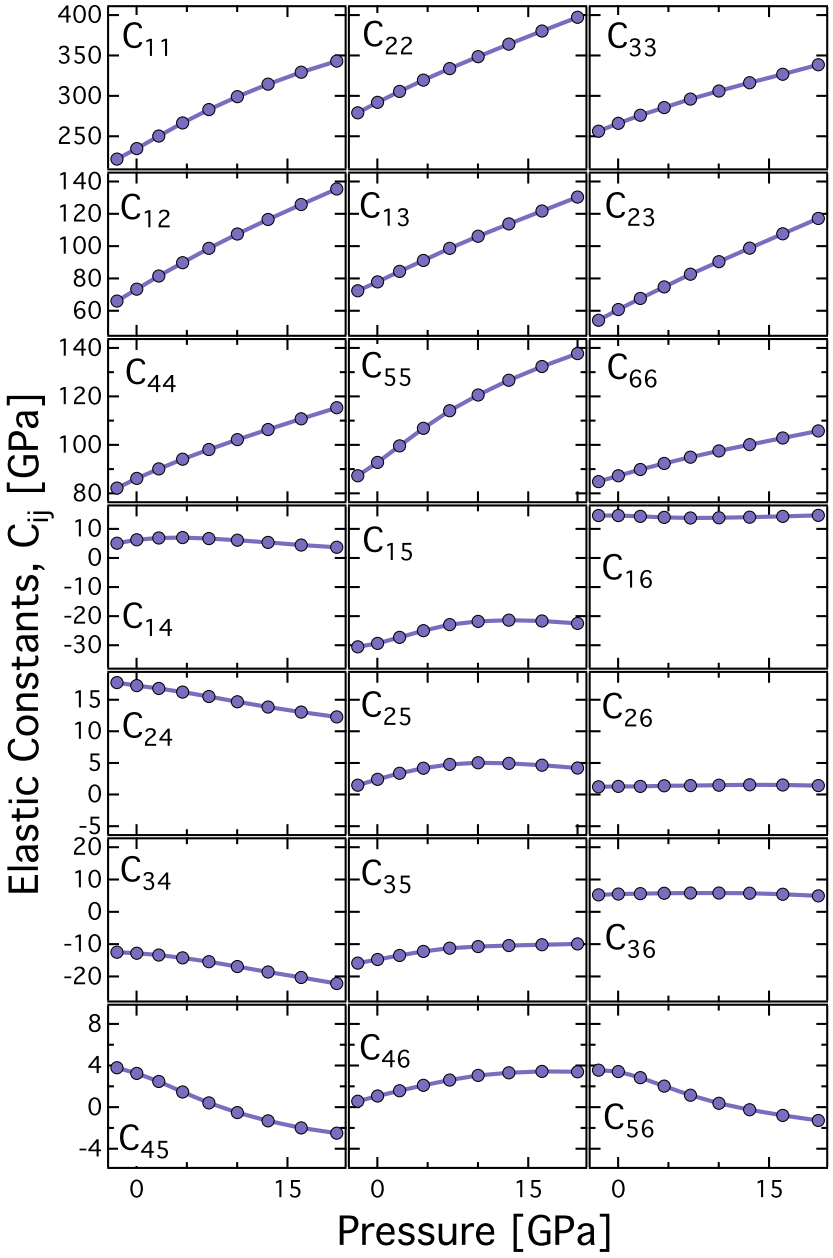

Fig. 4. Full elastic constant tensor (C_{ij}) components, for phase-Pi as a function of pressure (Table 2). There are 21 sub plots, representing the 21 independent elastic constants for the triclinic symmetry.

(Mookherjee et al., 2015; Hermann and Mookherjee, 2016). Hence, in the following sections, we will be considering physical properties unaffected by hydrogen bond symmetrization.

3.2. Equation of state and elasticity

Our results indicate that the static (0 K) zero-pressure unit-cell volume for the triclinic phase-Pi is V_0 ~310.34 (±0.03) Å^3. Unit cell volume predicted by PBE is ~0.7% larger than the zero-pressure volume based on single crystal X-ray diffraction study, V_0^{exp} (Wunder et al., 1993a,b; Daniels and Wunder, 1996). A third-order Birch-Murnaghan fit (Birch, 1978) to the energy vs. volume results yield a static (0 K) zero pressure bulk modulus (K_0) and pressure derivative of bulk modulus (K_0') as 133.12 (±0.37) GPa and 3.64 (±0.02) respectively (Fig. 3). Our static (0 K) results are in very good agreement with the previously reported high-pressure synchrotron X-ray diffraction experiment, K_0 of 133.13 GPa (Grevel et al., 2000). The predicted zero pressure lattice parameters are also in good agreement with the single crystal diffraction results with $a_0 > a_0^{exp}$ by 0.4%, $b_0 < b_0^{exp}$ by 0.3%, $c_0 > c_0^{exp}$ by 0.03%, $\alpha_0 < \alpha_0^{exp}$ by 0.5%, $\beta_0 < \beta_0^{exp}$ by 0.6%, and $\gamma_0 > \gamma_0^{exp}$ by 0.3% (Fig. 3). The angular lattice parameters β and γ are closer to 90°. Upon compression, β increases from 88.3° towards 90° whereas γ decreases from 93.2° towards 90° (Fig. 3). The angular lattice parameter α initially decreases from 115.15° to 115.09° upon compression till 7 GPa. At pressure >7 GPa α increases (Fig. 3). Thus, within its thermodynamic stability, i.e., 2–7 GPa, the angular lattice parameter α and γ decrease whereas, β increases. It is well known that the static (0 K) zero pressure volume prediction based on PBE is often greater and the predicted bulk modulus often softer in comparison to the experimental results. In contrast, the static (0 K) zero pressure volume prediction based on local density approximation (LDA) is often smaller and the predicted bulk modulus often stiffer compared to the experimental results (Mookherjee and Tsuchiya, 2015). We have incorporated the temperature effects on the bulk modulus using Gibbs2 (Otero-de-la-Roza et al., 2011), and find that the predicted bulk modulus at 300 K is ~131 GPa, i.e., 1.6% softer compared to the experimental results (Fig. 3) (Grevel et al., 2000). This softening in bulk modulus is similar to other hydrous phases such as amphibole (Mookherjee and Bezacier, 2012).

Phase-Pi has triclinic space group symmetry i.e., it has 21 independent elastic constants (Nye, 1985). All of the principal C_{11}, C_{22}, C_{33}, most of the off-diagonal, C_{ij} (where i≠j) and shear elastic constants, C_{44}, C_{55}, C_{66} stiffen i.e., $\frac{dC_{ij}}{dP} > 0$ (Fig. 4, Table 2). The C_{11} and C_{22} stiffens at a faster rate than C_{33} as noted by their pressure derivatives The off- diagonal elastic constants such as C_{16}, C_{24}, C_{34}, C_{45}, and C_{56} decreases upon compression, i.e., $\frac{dC_{ij}}{dP} < 0$. i.e., (Fig. 4, Table 2). The hill averaged bulk (K_H) and shear (G_H) modulus increase upon compression. Pressure dependence of full elastic constant tensor could be described by finite strain formulations as outlined in previous study (Chheda et al., 2014) and the finite strain fit parameters, such as C_{ij0} and its pressure derivatives C'_{ij0} $\left(\frac{dC_{ij}}{dP}\right)$ and C''_{ij0} $\left(\frac{d^2C_{ij}}{dP^2}\right)$ are reported in Table 2.

4. Discussion

The high-pressure elasticity of phase-Pi can be understood in terms of the crystal structure. In particular, the compressibility of the individual polyhedral units tends to determine the overall compressibility and elasticity of phase-Pi. There are four distinct crystallographic sites for the silicon atoms. The compressibility of TO_4 tetrahedral units for Si(1) and Si(2) are very similar with zero pressure bulk modulus ($K_O^{SiO_4}$) of 279 GPa, and pressure derivative of the bulk modulus ($K_O^{SiO_4\prime}$) of 8.6. The compressibility of TO_4 tetrahedral units for Si(3) and Si(4) are likewise similar with zero pressure bulk modulus ($K_O^{SiO_4}$) of 354 GPa, and pressure derivative of the bulk modulus ($K_O^{SiO_4\prime}$) of 4.9. In contrast to the TO_4 tetrahedral units, the MO_6 octahedral sites where M = Al are softer. There are six distinct crystallographic sites for the aluminum atoms. The compressibility of the respective MO_6 octahedral units relate as Al(1) ≅ Al(2), Al(3) ≅ Al(4), Al(5) ≅ Al(6), with zero pressure bulk modulus ($K_O^{AlO_6}$) and pressure derivative of the bulk modulus ($K_O^{AlO_6\prime}$) being 131 GPa, 6.3, 189 GPa, 6.4, and 175 GPa, 7.2, respectively. The Al(1) and Al(2) octahedra are significantly softer compared to the other octahedral units. This could be related to the fact that the

Table 2
The full elastic constant tensor (C_{ij}), bulk (K_H), and shear (G_H) modulus for phase-Pi as a function of pressure. The finite strain fit results are also tabulated. Subscript "H" refers to the "Hill" average.

V	315	310	305	300	295	290	285	280	Finite strain fit		
P	−2.0	0.0	2.2	4.6	7.2	10.0	13.1	16.4	C_{ij0}	C'_{ij0}	C''_{ij0}
C_{11}	221.7	234.8	250.2	266.5	282.9	299.1	314.5	329.1	234.6	7.2	−0.192
C_{12}	66.0	73.4	81.5	89.8	98.7	107.5	116.4	125.8	73.4	3.7	−0.070
C_{13}	72.4	77.9	84.4	91.1	98.7	106.2	113.8	121.7	77.8	3.1	−0.052
C_{14}	5.0	6.2	6.9	7.0	6.7	6.1	5.3	4.5	6.2	0.2	−0.041
C_{15}	−30.5	−29.4	−27.3	−25.0	−22.9	−21.8	−21.4	−21.7	−29.6	1.2	−0.090
C_{16}	14.6	14.6	14.3	14.0	13.8	13.8	14.0	14.3	14.6	−0.2	0.019
C_{22}	279.0	292.0	305.5	319.4	333.9	348.6	364.0	380.2	291.5	6.2	−0.122
C_{23}	54.2	60.7	67.6	74.8	82.6	90.4	98.7	107.6	60.6	3.2	−0.045
C_{24}	17.7	17.2	16.8	16.2	15.5	14.7	13.8	13.1	17.3	−0.2	−0.008
C_{25}	1.5	2.4	3.4	4.2	4.8	5.0	4.9	4.6	2.4	0.5	−0.042
C_{26}	1.2	1.3	1.3	1.4	1.4	1.5	1.5	1.5	1.3	0.0	−0.001
C_{33}	256.2	266.0	275.9	285.5	295.9	306.0	316.1	326.9	265.6	4.6	−0.121
C_{34}	−12.5	−12.8	−13.4	−14.3	−15.5	−16.9	−18.6	−20.3	−12.8	−0.3	−0.019
C_{35}	−15.9	−14.8	−13.5	−12.3	−11.3	−10.7	−10.4	−10.2	−14.7	0.6	−0.039
C_{36}	5.2	5.5	5.6	5.8	5.8	5.8	5.8	5.4	5.5	0.1	−0.013
C_{44}	82.2	86.1	90.0	94.0	98.1	102.2	106.4	110.8	86.0	1.8	−0.045
C_{45}	3.8	3.2	2.5	1.5	0.4	−0.5	−1.3	−2.0	3.3	−0.4	0.015
C_{46}	0.6	1.1	1.6	2.1	2.6	3.1	3.3	3.4	1.0	0.3	−0.016
C_{55}	87.3	92.8	99.6	106.8	114.0	120.6	126.7	132.3	92.4	3.4	−0.122
C_{56}	3.5	3.4	2.8	2.0	1.1	0.4	−0.3	−0.8	3.3	−0.3	0.009
C_{66}	84.9	87.3	89.8	92.4	94.9	97.5	100.1	102.9	87.2	1.2	−0.034
K_H	124.6	133.2	142.7	152.4	162.6	172.6	182.7	193.0	133.2	4.4	−0.098
G_H	86.4	90.1	94.1	98.1	102.1	105.8	109.5	113.0	90.1	1.9	−0.063

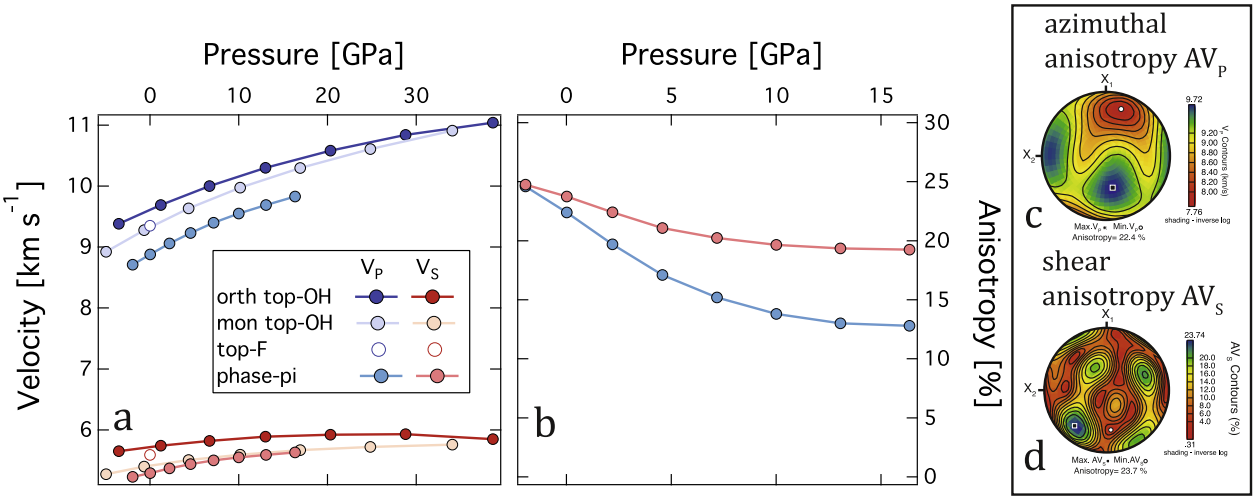

Fig. 5. (a) Pressure dependence of compressional wave (V_P) and shear wave velocity (V_S) for phase-Pi, topaz-OH (both orthorhombic and monoclinic structure), and topaz-F are shown. (b) Plot of elastic anisotropy AV_P and AV_S for phase-Pi as a function of pressure. (c–d) The stereographic projection down the X_3 axes for AV_P and AV_S at 0 GPa. The velocity (V_P) and difference (dV_S) color contours are also shown for reference.

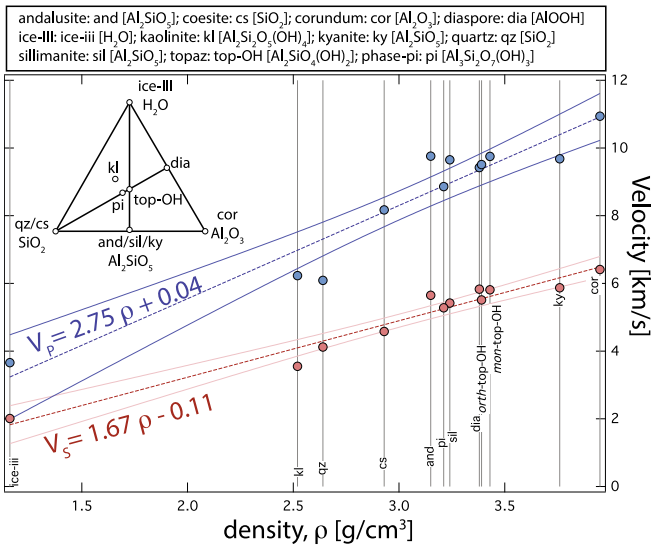

Fig. 6. Plot of V_P and V_S as a function of density for the mineral phases that are stable in subducted sediments. The blue and red dashed line represents linear regression fits for compressional wave and shear wave respectively. Inset shows a ternary plot of the Al_2O_3-SiO_2-H_2O components that are relevant for the mineral phases that are stable in subducted sediments (Table 3).

Al1-O12 and Al2-O11 bond lengths are significantly larger, rendering the octahedral sites more distorted. Note that O11 and O12 are part of the O–H groups involved in strong hydrogen bonds.

The compressional (V_P) and shear (V_S) wave velocities increase upon compression (Fig. 5). However, the V_P and V_S velocities of phase-Pi are slower than those of topaz-OH (Mookherjee et al., 2016) and the relation persists at higher pressures (Fig. 5). The P-wave azimuthal and S-wave anisotropy for phase-Pi is AV_P ~22.4% and AV_S ~23.7% at 0 GPa (Fig. 5). At pressures ~0 GPa, the fast direction of V_P is consistent with C_{33} being greater than C_{11} (Fig. 5).

Along a subduction zone significant amounts of sediments could be transported which are often hydrated. A simplified Al_2O_3-SiO_2-H_2O (ASH) ternary is a good representative of the alumina and silica rich layers (Wunder et al., 1993a,b; Schreyer, 1995). Along a typical cold geothermal gradient (~4 °C/km) hydrous aluminosilicates such as phase-Pi could be stable between a temperature and pressure range of 400 °C-700 °C and 2.0–7.0 GPa respectively. Along the cold geotherm, at lower temperatures of ~400 °C phase-Pi is formed via the reaction:

$$3\mathrm{AlOOH(diaspore)} + 2\mathrm{SiO_2(coesite)} = 1\mathrm{Al_3Si_2O_7(OH)_3(phase\text{-}Pi)} \quad (1)$$

where as, at the higher pressure limits of 7 GPa, phase-Pi decomposes via a reaction:

$$2\mathrm{Al_3Si_2O_7(OH)_3(phase\text{-}Pi)} = 3\mathrm{Al_2SiO_4(OH)_2(topaz\text{-}OH)} + 1\mathrm{SiO_2(coesite)} \quad (2)$$

Based on the zero pressure density, compressional (V_P) and shear (V_S) velocity of all the hydrous phases belonging to the ASH ternary

Table 3
Density, compressional (V_P), and shear (V_S) wave velocity of mineral phases in Al_2O_3-SiO_2-H_2O ternary.

Mineral	Abbreviation	Formula	ρ [g/cm^3]	V_P [km/s]	V_S [km/s]	References
Corundum	cor	Al_2O_3	3.95	10.94	6.41	Ohno et al. (1986)
Quartz	qz	SiO_2	2.64	6.09	4.12	Ohno et al. (2006)
Coesite	cs	SiO_2	2.93	8.17	4.58	Weidner and Carleton (1977)
Ice	ice-iii	H_2O	1.16	3.66	2.01	Tulk et al. (1994)
Andalusite	and	Al_2SiO_5	3.15	9.76	5.65	Vaughan and Weidner (1978)
Sillimanite	sil	Al_2SiO_5	3.24	9.65	5.42	Vaughan and Weidner (1978)
Kyanite	ky	Al_2SiO_5	3.76	9.68	5.87	Winkler et al. (2001)
Diaspore	dia	AlOOH	3.38	9.42	5.83	Jiang et al. (2008)
Kaolinite	kl	$Al_2Si_2O_5(OH)_4$	2.52	6.23	3.55	Katahara (1996)
Topaz	*mon*-top-OH	$Al_2SiO_4(OH)_2$	3.43	9.75	5.81	Mookherjee et al. (2016)
Topaz	*orth*-top-OH	$Al_2SiO_4(OH)_2$	3.39	9.51	5.51	Mookherjee et al. (2016)
Phase-Pi	pi	$Al_3Si_2O_7(OH)_3$	3.21	8.86	5.28	This study

(Fig. 6, Table 3), we gather that the formation of phase-Pi is likely to be associated with ΔV_P and ΔV_S of −0.67% and −0.95% respectively. The reduction of velocity is primarily owing to a lower velocity of phase-Pi compared to diaspore. The decomposition of phase-Pi is likely to be associated with ΔV_P and ΔV_S of 3.55% and −0.04% respectively. This is owing to the fact that V_P of topaz-OH and coesite is greater than phase-Pi whereas the average V_S of topaz-OH and coesite is almost equal or slightly less than phase-Pi. Hence, decomposition of phase-Pi is likely to be associated with an anti-correlation between the ΔV_P and ΔV_S. However, the presence of other hydrous phases may smear such diagnostic signature. Further information on the effect of temperature, anisotropy, petrographic fabric or lattice preferred orientations on the seismic velocity of hydrous aluminosilicate phases including phase-Pi will certainly aid in refining our prediction.

Acknowledgements

Authors thank two anonymous reviewers for their careful and constructive comments. Y.P., S.B., and M.M. acknowledge the US National Science Foundation grant (EAR-1634422). A.H. acknowledges UK National Supercomputing Service through the UKCP consortium (funded by United Kingdom, EPSRC Grant EP/K01465X) and project ID d56 'Planetary Interiors', and by the Condensed Matter Centre for Doctoral Training (funded by United Kingdom, EPSRC Grant 215 EP/L015110/1). AH also acknowledges Royal Society Research Grant RG150247. S. L. acknowledges USTC, China for funding the summer internship.

Appendix A. Supplementary data

Supplementary data associated with this article can be found, in the online version, at http://dx.doi.org/10.1016/j.pepi.2017.05.016.

References

Birch, F., 1978. Finite strain isotherm and velocities for single crystal and polycrystalline NaCl at high-pressures and 300 K. J. Geophys. Res. 83, 1257–1268.
Chheda, T., Mookherjee, M., Mainprice, D., dos Santos, A.M., Molaison, J.J., Chantel, J., Manthilake, G., Bassett, W.A., 2014. Structure and elasticity of phlogopite under compression: geophysical implications. Phys. Earth Planet. Int. 233, 1–12.
Daniels, P., Wunder, B., 1993. Crystal structure of trialuminium tri hydroxo disilicate, $Al_3Si_2O_7(OH)_3$. Z. Krist. 206, 103–105.
Daniels, P., Wunder, B., 1996. $Al_3Si_2O_7(OH)_3$, phase Pi (formerly piezotite): crystal structure of a synthetic high-pressure silicate rediscovered. Eur. J. Mineral. 8, 1283–1292.
Grevel, K.-D., Fasshauer, D.W., Rohling, S., 2000. Bulk moduli and *P-V-T* data of the high-pressure phases topaz-OH, $Al_2SiO_4(OH)_2$, and phase Pi, $Al_3Si_2O_7(OH)_3$. J. Conf. Abstracts, 5, 1, EMPG VIII, http://www.the-conference.com/JConfAbs/5/44.html.
Hermann, A., Mookherjee, M., 2016. High-pressure phase of brucite stable at Earth's mantle transition zone and lower mantle conditions. Proc. Natl. Acad. Sci. 113 (49), 13971–13976.
Hirschmann, M., 2006. Water, melting, and the deep Earth H_2O cycle. Ann. Rev. Earth. Planet. Sci. 34, 629–653.
Hohenberg, P., Kohn, W., 1964. Inhomogeneous electron gas. Phys. Rev. B 136, B864–B871.
Ichikawa, H., Kawai, K., Yamamoto, S., Kameyama, M., 2015. Effect of water on subduction of continental materials to the deep Earth. In: Khan, A., Deschamps, F. (Eds.), The Earth's Heterogenous Mantle, pp. 275–299.
Jiang, F., Majzlan, J., Speziale, S., He, D., Duffy, T.S., 2008. Single-crystal elasticity of diaspore, AlOOH, to 12 GPa by brillouin scattering. Phys. Earth. Planet. Int. 170, 221–228.
Katahara, K.W., 1996. Clay mineral elastic properties. SEG Ann. Meet. Expanded abs., 1691–1694 http://dx.doi.org/10.1190/1.1826454.
Kawamoto, T., 2006. Hydrous phases and water transport in the subducting slab. Rev. Min. Geochem. 62, 85–116.
Kohn, W., Sham, L.J., 1965. Self-consistent equations including exchange and correlation effects. Phys. Rev. 140, A1133–A1138.
Kresse, G., Furthmüller, J., 1996a. Efficiency of ab-initio total energy calculations for metals and semiconductors. Comput. Mat. Sci. 6, 15–50.
Kresse, G., Furthmüller, J., 1996b. Efficient iterative schemes for ab initio total-energy calculations using plane-wave basis set. Phys. Rev. B 54, 11169–11186.
Kresse, G., Hafner, J., 1993. Ab initio molecular dynamics for liquid-metals. Phys. Rev. B 47, 558–561.
Kresse, G., Joubert, D., 1999. From ultrasoft pseudopotentials to the projector augmented-wave method. Phys. Rev. B 59, 1758–1775.
Mainprice, D., 1990. An efficient FORTRAN program to calculate seismic anisotropy from the lattice preferred orientation of minerals. Comput. Gesosci. 16, 385–393.
Mei, S., Kohlstedt, D.L., 2000. Influence of water on plastic deformation of olivine aggregates 1. Diffusion creep regime. J. Geophys. Res. 105, 21457–21469.
Monkhorst, H.J., Pack, J.D., 1976. Special points for Brillouin-zone integrations. Phys. Rev. B 13, 5188–5192.
Mookherjee, M., 2014. High-pressure elasticity of sodium majorite garnet, $Na_2MgSi_5O_{12}$. Am. Mineral. 99, 2416–2423.
Mookherjee, M., Bezacier, L., 2012. The low velocity later in subduction zone: structure and elasticity of glaucophane at high pressures. Phys. Earth Planet. Int. 208–209, 50–58.
Mookherjee, M., Mainprice, D., 2014. Unusually large shear wave anisotropy for chlorite in subduction zone settings. Geophys. Res. Lett. 41, 1506–1513.
Mookherjee, M., Tsuchiya, J., 2015. Elasticity of superhydrous phase, B, $Mg_{10}Si_3O_{10}(OH)_4$. Phys. Earth Planet. Int. 238, 42–50.
Mookherjee, M., Speziale, S., Marquardt, H., Jahn, S., Koch-Müller, M., Liermann, H.-P., 2015. Equation of state and elasticity of the 3.65 Å phase- implications for the X-discontinuity. Am. Mineral. 100, 2199–2208.
Mookherjee, M., Tsuchiya, J., Hariharan, A., 2016. Crystal structure, equation of state, and elasticity of hydrous aluminosilicate phase, topaz-OH $(Al_2SiO_4(OH)_2)$ at high pressures. Phys. Earth Planet. Int. 251, 24–35.
Morris, J., Tera, F., 1989. ^{10}Be and ^{9}Be in mineral separates and whole rocks from volcanic arcs: implications for sediment subduction. Geochim. Cosmochim. Acta 53, 3197–3206.
Nye, J.F., 1985. Physical Properties of Crystals. Oxford University Press, Clarendon.
Ohno, I., Harada, K., Yoshitomi, C., 2006. Temperature variation of elastic constants of quartz across the α–β transition. Phys. Chem. Mineral. 33, 1–9.
Ohno, I., Yamamoto, S., Anderson, O.L., Noda, J., 1986. Determination of elastic constants of trigonal crystals by the rectangular parallelepiped resonance method. J. Phys. Chem. Solids. 47, 1103–1108.
Ono, S., 1998. Stability limits of hydrous minerals in sediment and mid-ocean ridge basalt compositions: implications for water transport in subduction zones. J. Geophys. Res. 103, 18253–18267.
Ono, S., 1999. High temperature stability of phase egg, $AlSiO_3(OH)$ Contrib. Mineral. Petrol. 137, 83–89.
Otero-de-la-Roza, A., Abbasi-Perez, D., Launa, V., 2011. Gibbs2: A new version of the quasiharmonic model code. II. Models for solid-state thermodynamics, features and implementation Comp. Phys. Comm. 182, 2232–2248.
Peacock, S.M., 1990. Fluid processes in subduction zones. Science 248, 329–337.
Perdew, J.P., Burke, K., Erzerhof, M., 1996. Generalized gradient approximation made simple. Phys. Rev. Lett. 77, 3865–3868.
Plank, T., Langmuir, C.H., 1993. Tracing trace elements from sediment input to volcanic output at subduction zones. Nature 326, 739–742.
Rea, D.K., Ruff, L.J., 1996. Composition and mass flux of sediment entering the world's subduction zones: Implications for global sediment budgets, great earthquakes, and volcanisums. Earth Planet. Sci. let. 140, 1–12.
Schmidt, M.W., Finger, L.W., Angel, R.J., Robert, E., 1998. Synthesis, crystal structure and phase relations of $AlSi_3OH$, a high pressure hydrous phase. Am. Mineral 83, 881–888.
Schreyer, W., 1995. Ultradeep metamorphic rocks: the retrospective viewpoint. J. Geophys. Res. 100, 8353–8366.
Smyth, J., 2006. Hydrogen in high-pressure silicate and oxide mineral structures. Rev. Min. Geochem. 62, 85–116.
Tera, F., Brown, L., Morris, J., Sacks, I.S., Klein, J., Middleton, R., 1986. Sediment incorporation in island arc magmas: inferences from ^{10}Be. Geochim. Cosmochim. Acta 50, 636–660.
Tsuchiya, J., Mookherjee, M., 2015. Crystal structure, equation of state, and elasticity of phase H($MgSiO_4H_2$) at Earth's lower mantle pressure. Sci. Rep. 5, 15534.
Tsuchiya, J., Tsuchiya, T., Tsuneyuki, S., Yamanaka, T., 2002. First principles calculation of a high-pressure hydrous phase, δ-AlOOH. Geophys. Res. Lett. 29, 1909.
Tsuchiya, J., Tsuchiya, T., Tsuneyuki, S., 2005. First-principles study of hydrogen bond symmetrization of phase D under high pressure. Am. Mineral. 90, 44–49.
Tulk, C.A., Gagnon, R.E., Kiefte, H., Clouter, M.J., 1994. Elastic constants of ice III by brillouin spectroscopy. J. Chem Phys. 101, 2350.
Vaughan, M.T., Weidner, D.J., 1978. The relationship of elasticity and crystal structure in andalusite and sillimanite. Phy. Chem. Mineral. 3, 133–144.
Weidner, D.J., Carleton, H.R., 1977. Elasticity of coesite. J. Geophys. Res. 82, 1334–1346.
White, W.M., Dupre, B., 1986. Sediment subduction and magma genesis in the Lesser Antilles: isotopic and trace element constraints. J. Geophys. Res. 91, 5927–5941.
Winkler, B., Hytha, M., Warren, M.C., Milman, V., Gale, J.D., Schreuer, J., 2001. Calculation of the elastic constants of the Al2SiO5 polymorphs andalusite, silimanite and kyanite. Z. Kristallogr. 216, 67–70.
Wunder, B., Medenbach, O., Krause, W., Schreyer, W., 1993a. Synthesis, properties and stability of $Al_3Si_2O_7(OH)_3$ (phase Pi), a hydrous high-pressure phase in the system Al_2O_3-SiO_2-H_2O (ASH). Eur. J. Mineral. 5, 637–649.
Wunder, B., Rubie, D.C., RossII, C.R., Medenbach, O., Seifert, F., Schreyer, W., 1993b. Synthesis, stability, and properties of $Al_2SiO_4(OH)_2$: a fully hydrated analogue of topaz. Am. Mineral. 78, 285–297.